

Computation and analysis of the characteristic spectra of Eu(II) ions in single-bubble sonoluminescence

Xue-Ping Wang(王学坪) and Jin-Fu Liang(梁金福)

Citation: Chin. Phys. B, 2025, 34 (**9**): 094301. DOI: 10.1088/1674-1056/addaa1
http://cpb.iphy.ac.cn; http://iopscience.iop.org/cpb

What follows is a list of articles you may be interested in

Effect of metal plate on ultrasonic cavitation field distribution

Jin-He Liu(刘金河), Zhuang-Zhi Shen(沈壮志), Peng-Fei Cao(曹鹏飞), Jian-Feng Li(李建锋), and Xiao-Qiang Bai(白小强)
Chin. Phys. B, 2025, 34 (**5**): 054302. DOI: 10.1088/1674-1056/adca9d

Overcoming bandwidth limitations in space-coiled acoustic metamaterials through inclined perforated plate design

Jixin Liu(刘继鑫), Fengmin Wu(吴丰民), Ting Li(李婷), Junjun Wang(王军军), Xinye Zou(邹欣晔), and Dong Zhang(章东)
Chin. Phys. B, 2025, 34 (**1**): 014303. DOI: 10.1088/1674-1056/ad8fa2

Lamb wave TDTE super-resolution imaging assisted by deep learning

Liu-Jia Sun(孙刘家), Qing-Bang Han(韩庆邦), and Qi-Lin Jin(靳琪琳)
Chin. Phys. B, 2025, 34 (**1**): 014301. DOI: 10.1088/1674-1056/ad886d

Acoustic radiation force on a cylindrical composite particle with an elastic thin shell and an internal eccentric liquid column in a plane ultrasonic wave field

Rui-Qi Pan(潘瑞琪), Zhi-Wei Du(杜芷玮), Cheng-Hui Wang(王成会), Jing Hu(胡静), and Run-Yang Mo(莫润阳)
Chin. Phys. B, 2024, 33 (**9**): 094302. DOI: 10.1088/1674-1056/ad5d66

Behaviors of cavitation bubbles driven by high-intensity ultrasound

Chen-Yang Huang(黄晨阳), Fan Li(李凡), Shi-Yi Feng(冯释毅), Cheng-Hui Wang(王成会), Shi Chen(陈时), Jing Hu(胡静), Xin-Rui He(何芯蕊), and Jia-Kai Song(宋家凯)
Chin. Phys. B, 2024, 33 (**2**): 024301. DOI: 10.1088/1674-1056/ad0717

Computation and analysis of the characteristic spectra of Eu(II) ions in single-bubble sonoluminescence

Xue-Ping Wang(王学坪) and Jin-Fu Liang(梁金福)†

School of Physics and Electronic Science, Guizhou Normal University, Guiyang 550025, *China*

(Received 5 March 2025; revised manuscript received 18 May 2025; accepted manuscript online 20 May 2025)

Single-bubble sonoluminescence (SBSL) occurs when a tiny bubble with an extremely small volume, isolated within a liquid, periodically compresses and expands in response to a strong ultrasonic field, emitting a brief burst of bright light. Sonoluminescence spectroscopy serves as a powerful tool for analyzing the material structure and physical state of these bubbles. Recent experimental results have demonstrated that the sonoluminescence spectra of moving single bubbles exhibit the characteristic spectra of divalent europium ions [Eu(II)] in solutions containing europium chloride ($EuCl_2$). To elucidate the radiation mechanism of the characteristic spectra of Eu(II) ions during sonoluminescence, we combined fluid mechanics, the Keller–Miksis (KM) equation, and spectral equations to calculate the spectral intensity and radiation power of SBSL in $EuCl_2$ solutions, as well as the spatial distributions of temperature, pressure, particle number density, ionization energy, ionization degree and opacity within bubbles. The results indicate that the characteristic spectra of Eu(II) ions may arise from the transition radiation excited under a localized environment of high temperature, pressure, and density within bubbles. These findings could enhance our understanding of the mechanisms underlying sonoluminescence and potentially aid in the development of advanced diagnostic tools for analyzing high-energy processes in fluids.

Keywords: single-bubble sonoluminescence, Eu(II) characteristic spectrum, transition radiation

PACS: 43.35.+d, 78.60.Mq, 47.55.dd

DOI: 10.1088/1674-1056/addaa1 **CSTR:** 32038.14.CPB.addaa1

1. Introduction

When a solitary bubble immersed within a fluid experiences powerful compression from ultrasonic waves, it undergoes a swift implosion, leading to the phenomenon known as single-bubble sonoluminescence (SBSL).[1–3] This process is characterized by stable, spatially localized, and time-synchronized pulsating luminescence. During the collapse of the bubble, its internal environment becomes extremely extreme, with pressures reaching thousands of megapascals and temperatures soaring to about 10^4 K.[4] This triggers picosecond-level visible light flickering in the bubble and creates a transient plasma state in an instant, providing favorable conditions for ion excitation inside it.[5–9] This study analyzes the mechanism of spectral line emission from nonvolatile substances originating from the main liquid into the bubble.

Lanthanide ions (Ln^{n+}) are extensively studied and used in fields such as energy, biomedical imaging, and laser technology owing to their high excited-state lifetime and radiation conversion efficiency.[10] When lanthanide ions are doped into a bubble-forming liquid, the resulting sonoluminescence exhibits more pronounced and stable luminescence. In recent years, Ln(III) ions have been used as sonoluminescence probes, with several research groups recording characteristic spectral bands of many Ln(III) ions in aqueous solutions,[11–15] and the moving SBSL (m-SBSL) spectral bands of colloidal suspensions containing these ions.[16] To date, the only documented observation of sonochemiluminescence in Ln(II) compounds has been conducted by Gareev *et al*., who investigated the behaviors of Eu(II) and Sm(II) ions during the ultrasound-induced reductions of Eu(III) and Sm(III) in ethylene glycol.[17,18] In their pioneering work, Gareev *et al*. successfully identified the luminescent bands associated with Eu(II) ions in the m-SBSL spectra of dodecane suspensions containing nanoparticles of $EuCl_2$, $EuBr_2$, and $EuSO_4$. These luminescent bands correspond to the photoluminescence spectra of Eu(II) ions (specifically pertaining to the $4f^6 5\,d^1 \rightarrow 4f^7$ electronic transitions), exhibiting maximum luminescence peaks at the wavelengths of 404 nm, 413 nm, and 377 nm, respectively. The sonoluminescence bands arise from the introduction of nanoparticles during the deformation of the bubble, while the excitation of the Eu(II) luminescence center is attributed to the collisions between these nanoparticles and charged particles, predominantly electrons, which are periodically emitted from the core of the plasma under non-equilibrium thermal conditions.[19]

To elucidate the radiation mechanism of the characteristic spectra of Eu(II) ions and obtain detailed information about the conditions inside a bubble during the sonoluminescence process, we used an SBSL model. This model incorporates the effects of thermal and mass diffusion between the two gases present within a bubble, namely the inert gas and water vapor. It also considers the thermal exchange between the bubble's gas and the enveloping fluid, as well as the processes of

†Corresponding author. E-mail: jfliang@gznu.edu.cn

© 2025 Chinese Physical Society and IOP Publishing Ltd. All rights, including for text and data mining, AI training, and similar technologies, are reserved.

evaporation and condensation of water vapor at the bubble's interface. Additionally, the model accounts for chemical reactions and ionization phenomena occurring within a bubble. By employing the Keller–Miksis (KM) equation to define the boundary condition, we numerically solved the dynamic equations governing the fluid mechanics of the gas within a bubble. In this way, we were able to ascertain the distributional characteristics of pressure and temperature within a single bubble immersed in an aqueous $EuCl_2$ solution. Moreover, we derived the spatial distributions for spectral intensity, radiation power, particle number density, ionization energy, the degree of ionization, and opacity within the SBSL. This was achieved by integrating contributions from bremsstrahlung emitted by electron-neutral atom interactions, attachment radiation resulting from electron interactions with atoms or molecules, recombination radiation, and line spectral radiation from Eu(II) ions.

2. Theoretical model

The SBSL model adopted in this study is similar to those reported in previous studies.[7,9,20,21] In the theoretical model, equation (1) serves as the boundary condition governing the movement of the bubble wall, while a system of partial differential equations derived from fluid mechanics [Eq. (2)] is employed to elucidate the dynamic characteristics of the gas contained within the bubble. By coupling Eqs. (1) and (2) and applying numerical calculation methods, we can accurately simulate the bubble's internal temperature and pressure patterns at various temporal intervals.

The KM equation describes the radial motion of the bubble wall, considering the liquid's compressibility:[22–24]

$$(1-M)R\ddot{R}+\frac{3}{2}\left(1-\frac{M}{3}\right)\dot{R}^2=(1+M)\frac{1}{\rho_{\rm l}}(p_{\rm l}-p_\infty-p_{\rm s}(t+t_{\rm R}))+\frac{t_{\rm R}}{\rho_{\rm l}}\dot{p}_{\rm l}, \tag{1}$$

where R is the bubble radius, M is the Mach number at the bubble's boundary, representing the effects of the liquid's compressibility, $p_{\rm l}$ and $\rho_{\rm l}$ are the pressure and density at the fluid phase of the bubble's boundary, respectively. Additionally, p_∞ is the environmental pressure, $p_{\rm s}(t)$ is the driving acoustic pressure, and $t_{\rm R}=R/c_{\rm l}$, where $c_{\rm l}$ is the sound speed at the fluid.

In this study, we considered only bubble containing two types of gaseous constituents, namely argon and water vapor. According to the basic theory of compressible fluid mechanics, considering the mass and thermal diffusion processes between gases as well as the viscosity of gases, and assuming that bubble has spherical symmetry, the forms of the fluid mechanics partial equations satisfied by argon and water vapor within the bubble in the spherical coordinate system are[7,25]

$$\begin{aligned}
&\frac{\partial\rho_{\rm l}}{\partial t}+\frac{1}{r^2}\frac{\partial}{\partial r}\left[r^2(\rho_{\rm l}\upsilon+J_{\rm l})\right]=0,\\
&\frac{\partial\rho}{\partial t}+\frac{1}{r^2}\frac{\partial}{\partial r}(r^2\rho\upsilon)=0,\\
&\frac{\partial(\rho\upsilon)}{\partial t}+\frac{1}{r^2}\frac{\partial}{\partial r}(r^2\rho\upsilon^2)+\frac{\partial p}{\partial r}=\frac{1}{r^2}\frac{\partial}{\partial r}(r^2\tau_{rr})+\frac{\tau_{rr}}{r},\\
&\frac{\partial E}{\partial t}+\frac{1}{r^2}\frac{\partial}{\partial r}\left\{r^2[(E+p)\upsilon+q]\right\}=\frac{1}{r^2}\frac{\partial}{\partial r}(r^2\upsilon\tau_{rr}),
\end{aligned} \tag{2}$$

where t represents time, r represents the distance to the bubble's core, ρ_1 is the density of water vapor, ρ_2 is the density of the inert gas, $\rho=\rho_1+\rho_2$ is the total density of the gas, v is the average velocity of the gas within the bubble, J_1 is the mass flux of water vapor under the average velocity, p is the pressure of the gas, q is the energy flux due to thermal motion, τ_{rr} is the normal viscous stress, and E is the total energy of the gas.

When a sonoluminescent bubble collapses abruptly, the internal pressure and temperature rise abruptly to extreme levels, causing the gas to decompose, leading to the formation of many chemical species. The mass-action law was employed to model the chemical reactions and ionization processes occurring within the bubble. For simplicity, four chemical reaction processes were considered, including atomic and molecular ionization processes, as well as atomic or molecular electron adsorption processes[7]

$$\mathrm{H_2O}\leftrightarrow\mathrm{OH+H}, \tag{3}$$
$$\mathrm{OH}\leftrightarrow\mathrm{O+H}, \tag{4}$$
$$\mathrm{O+O}\leftrightarrow\mathrm{O_2}, \tag{5}$$
$$\mathrm{H+H}\leftrightarrow\mathrm{H_2}, \tag{6}$$
$$M\leftrightarrow M^+ +\mathrm{e}, \tag{7}$$
$$M+\mathrm{e}\leftrightarrow M^-, \tag{8}$$

where M represents Ar atoms and other atoms or molecules appearing in Eqs. (3)–(6), M^- stands for negatively charged ions such as H^-, O^-, O_2^-, *etc*. The radiation-related processes involving interactions of electrons with atoms, molecules, or ions can be described as follows:

$$\mathrm{O+e}\leftrightarrow\mathrm{O^-}+h\nu, \tag{9}$$
$$\mathrm{H+e}\leftrightarrow\mathrm{H^-}+h\nu, \tag{10}$$
$$\mathrm{O_2+e}\leftrightarrow\mathrm{O_2^-}+h\nu, \tag{11}$$
$$\mathrm{OH+e}\leftrightarrow\mathrm{OH^-}+h\nu. \tag{12}$$

The chemical equilibrium constant is obtained by using the theory of statistical thermodynamics, and the chemical reaction is calculated based on the equilibrium constant. In

chemical reactions of the form $A \leftrightarrow B + C$, the equilibrium constant K is

$$K = \frac{n_B n_C}{n_A}, \tag{13}$$

where n_i $(i = A, B, C)$ represents the molecular number density of gas. Owing to the high pressure when the chemical reaction occurs inside the bubble, the particle concentration inside the bubble approaches the limit value of $1/b$. According to Ref. [26], the modified chemical equilibrium constant is

$$K_p = K\left(1 - \frac{Nb}{V}\right)\exp\left(-\frac{Nb}{V - Nb}\right), \tag{14}$$

where V represents the volume of the bubble, N is the total number of particles within the bubble, and b is the van der Waals hard core volume.

By integrating over the relevant wavelength λ, the total radiated power is

$$P(t) = \int_{360\ \mathrm{nm}}^{430\ \mathrm{nm}} P(\lambda, t)\,\mathrm{d}\lambda. \tag{15}$$

The radiation power function, which is the overall power radiated by the bubble at wavelength λ per period, is derived from Ref. [7]

$$P(\lambda, t) = 8\pi^2 \int_0^R \int_{-1}^1 k_\lambda(r) P_\lambda^{\mathrm{PI}}(r) \times \exp\left(-\int_{r_x}^{R^2 - r^2(1-x^2)} k_\lambda \,\mathrm{d}s\right) r^2 \mathrm{d}r\,\mathrm{d}x, \tag{16}$$

where $P_\lambda^{\mathrm{PI}}(r)$ is the Planck radiation intensity, and k_λ is the absorption coefficient of spectral line emission; in the case of Eu(II), this coefficient is defined as

$$k_\lambda = \frac{\lambda^5}{2hc^2}\left[\exp\left(hc/\lambda kT\right) - 1\right] P_\lambda. \tag{17}$$

This paper mainly focuses on the $4f^7 6p \rightarrow 4f^7 6s$ transition of Eu(II) ions (see Fig. 1).[27,28] For the linear emission of Eu(II) ions, we hypothesize that the formation of excited Eu(II) ions in a single luminescent bubble during single-bubble sonoluminescence is mainly due to the thermal excitation. The radiated power per unit volume for state transition $i \rightarrow j$ can be calculated as follows:

$$P_{i,j} = \frac{n_{\mathrm{a}} g_i \mathrm{e}^{-E_i/kT}}{\sum g_i / kT} A_{i,j} h\nu_{i,j}, \tag{18}$$

where n_{a} represents the density number of the Eu(II) ions within the bubble; in this case, we set the number density of the Eu(II) ions to 10^{-5} of the overall particle number within the bubble. Moreover, g_i is the Lande factor of the i-th energy level E_i, $A_{i,j}$ is the transition probability,[27,28] and $h\nu_{i,j}$ is the photo energy.

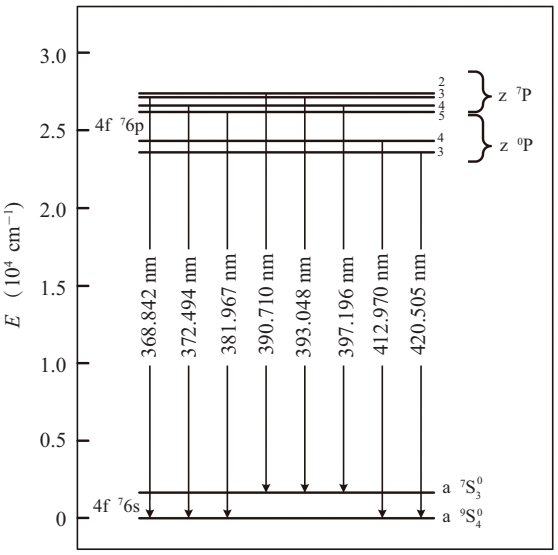


Fig. 1. Eu(II) ion transition.

Assuming that the spectral intensity emitted during SBSL is uniformly distributed, the radiation power per unit volume of the Eu(II) radical within a specified wavelength interval can be computed using the following equation:

$$P_\lambda \,\mathrm{d}\lambda = P_{i,j} g_{i,j}\left(\nu = \frac{c}{\lambda}\right)\frac{c}{\lambda^2}\,\mathrm{d}\lambda, \tag{19}$$

where ν is the emission frequency and $g_{i,j}$ is the Lorentz function, defined as

$$g_{i,j}(\nu) = \pi \frac{\Delta\nu/2}{(\nu - \nu_{i,j})^2 + (\Delta\nu/2)^2}, \tag{20}$$

where $\Delta\nu$ is the collision spread and resonance spread of the spectral lines,[29]

$$\Delta\nu = \sigma_0 v_0 n/\pi + 50\frac{n_{\mathrm{a}} f_{\mathrm{a}}}{\nu_{i,j}}, \tag{21}$$

where σ_0 is the collision cross-section, which is determined based on the diameter of the gas molecules.

Finally, the total energy radiated from the sonoluminescent bubble from time 0 to t during every sound cycle is given by

$$E_\lambda(t) = \int_0^t P(\lambda, t')\mathrm{d}t', \quad 0 \le t \le \frac{2\pi}{\omega}. \tag{22}$$

As SBSL is present, it is only during this short period of time that $P(\lambda, t')$ does not disappear.

3. Results and discussion

3.1. Physical process of bubble luminescence

In this study, certain parameters from the experiment conducted by Gareev *et al.*[19] were referenced in the numerical calculations; however, R_0 and other parameters were not provided in the paper. Therefore, our calculations are considered "conceptual calculations" and cannot be directly compared with the data obtained from the experimental procedure. The parameters used in our calculations are listed in Table 1.

Table 1. Simulation parameters. The unit 1 atm = 1.01325×10^5 Pa.

Symbol	Definition (value)
T_0	liquid temperature (273.15 K)
R_0	initial radius of the bubble (4.8 μm)
$\dot{R}(0)$	initial velocity of the bubble wall (0 m·s^{-1})
f	ultrasound frequency (27.0 kHz)
P_a	driving sound pressure amplitude (1.2731 atm)
p_∞	environmental pressure (1.0 atm)
η	liquid viscosity coefficient (1.01×10^{-3} Pa·s)
c_l	speed of sound (1483.0 m·s^{-1})
ρ_l	liquid density (1000.0 kg·m^{-3})
σ	surface tensile strength (0.07275 N·m^{-1})

To understand the mechanism of plasma generation within a bubble during the SBSL phenomenon, we conducted a simulation of the photoemission process within an argon bubble in a solution containing $EuCl_2$ at 0 °C. This simulation allowed us to observe the behavior of the bubble under specific conditions in great detail. A sound pressure amplitude at 1.2731 atm was employed to drive the bubble, simulating the actual SBSL conditions. To predict more accurately the characteristic peaks of Eu(II) ions in the SBSL emission spectrum, we postulated that these peaks result from light emitted by Eu(II) ions produced inside the bubble owing to thermal excitation. In addition, we set the number density of Eu(II) ions to 10^{-5} of the overall particle number within the bubble. This approach enabled us to approximate quantitatively the Eu(II) peaks within the SBSL spectrum range. As the bubble is compressed, it heats the internal gas and emits a flash; accordingly, we evaluated the radiation pulse of each flash and the changes in the bubble radius over time (see Fig. 2(a)). We then selected five moments during the flash (labeled points A–E) to evaluate the internal bubble conditions such as temperature, pressure, and the spectral characteristics of the transition radiation pertaining to Eu(II). The internal temperature and pressure increase considerably as the bubble collapses during compression, and after the peak radiation, both temperature and pressure decrease rapidly [Figs. 2(b) and 2(c)]. Furthermore, at each evaluated time point, the core of the bubble experiences the maximum temperature, which decreases abruptly as it approaches the bubble's perimeter [Fig. 2(b)]. It is observed that the bubble's internal pressure is evenly distributed throughout [Fig. 2(c)]. This occurs because when a bubble is compressed, the thermal movements of the gas molecules inside it increases owing to the temperature rise, leading to the rapid diffusion of heat within the bubble. This rapid thermal transfer contributes to an even distribution of pressure within the bubble, as the transfer of heat reduces the temperature difference between different regions within the bubble. In addition, when a bubble bursts, the fluid undergoes compression or dilation due to the internal pressure of the bubble. The compressibility of a liquid determines how much its volume changes with pressure. Within the bubble, the compressibility of the liquid helps equalize the pressure in different areas; the liquid can compress in regions wherein the pressure is higher and expand in regions wherein the pressure is lower, thus allowing the pressure to achieve a relatively uniform state. From point A to point D, the radiation spectrum accumulates over time as the radiation power increases, leading to an increase in the total intensity [Fig. 2(a)]. Within the wavelength region of 0.36 μm to 0.43 μm, the spectral peaks of Eu(II) gradually fade into the continuous spectrum's backdrop and ultimately disappear [Fig. 2(d)].

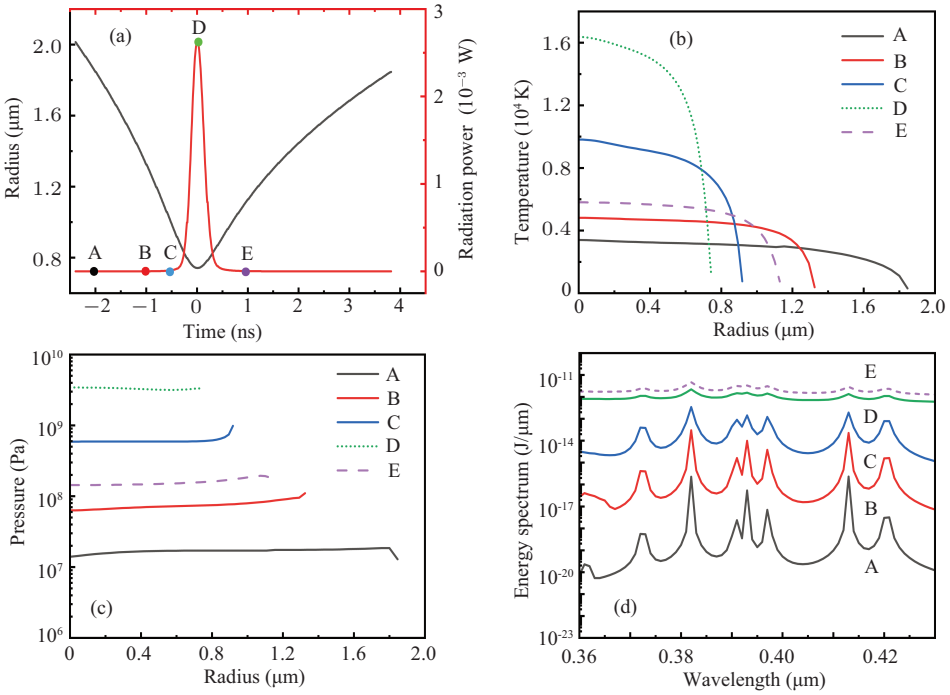


Fig. 2. Ar bubble in an $EuCl_2$ solution at 0 °C at the driving sound pressure amplitude of 1.2731 atm: (a) evolution of bubble radius and radiated power over time, (b) relationship between temperature and radius, (c) relationship between pressure and radius, (d) energy spectrum.

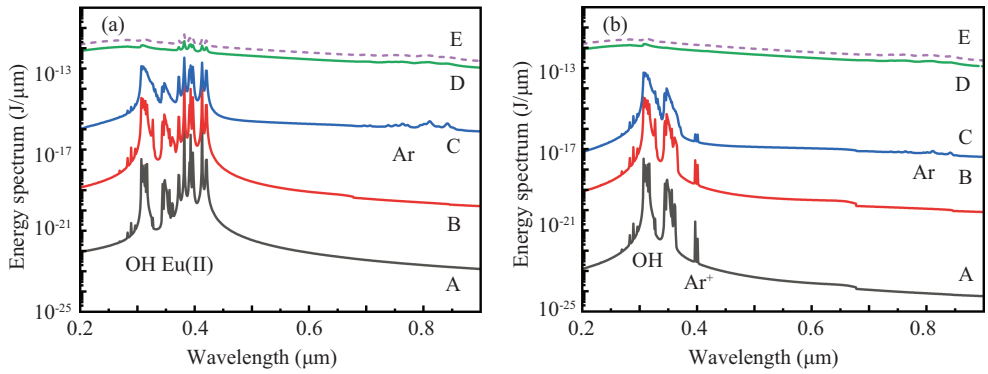


Fig. 3. Ar bubble sonoluminescence spectra within the range of 0.2 μm–0.9 μm. (a) Spectra obtained in the presence of $EuCl_2$ solution. (b) Spectra obtained in the absence of $EuCl_2$ solution. The black, red, blue, green, and purple lines correspond to the different moments. The amplitude of the driving sound pressure is 1.2731 atm.

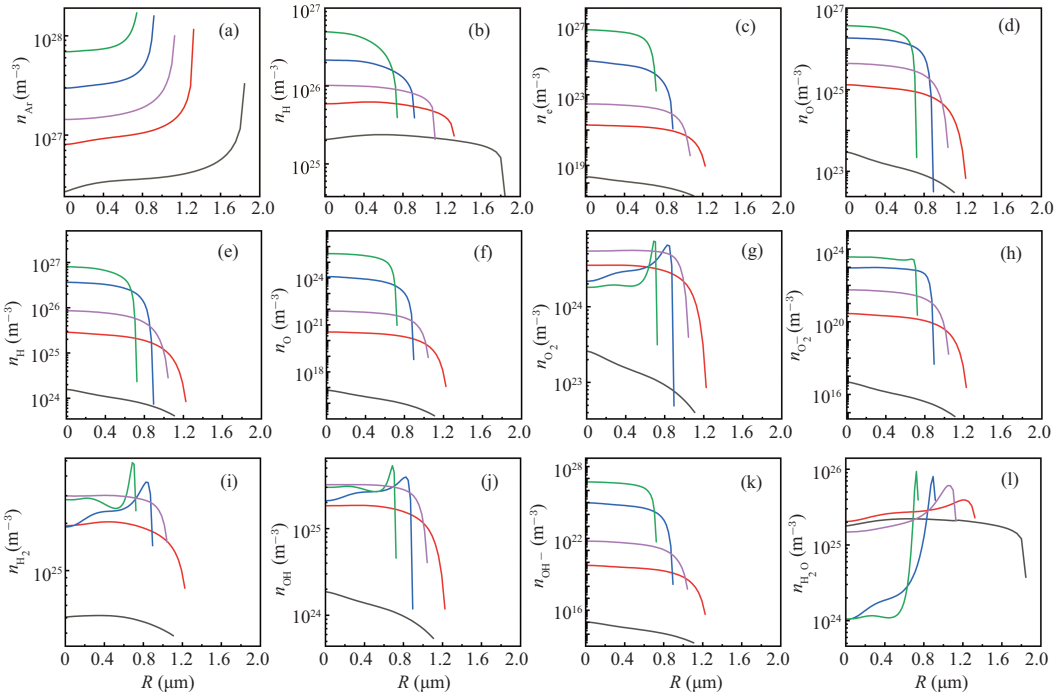


Fig. 4. Spatial distributions of densities calculated for different particles: (a) Ar, (b) H^-, (c) e^-, (d) O, (e) H, (f) O^-, (g) O_2, (h) O_2^-, (i) H_2, (j) OH, (k) OH^-, and (l) H_2O. The black, red, blue, green, and purple lines correspond to specific moments A, B, C, D, and E indicated in Fig. 2(a).

During the process of Eu(II) excitation inside a bubble with argon and water gas, the OH, Ar, and Ar^+ may be excited. We calculated the Ar spectra of a bubble (within the wavelength range of 0.2 μm–0.9 μm) with and without an $EuCl_2$ solution. It can be observed that the variation trends of the OH line spectra and the Eu(II) ion line spectra within the range of 0.30 μm–0.36 μm are approximately the same. However, the Ar atomic line spectrum in the range of 0.68 μm–0.88 μm becomes obvious at time E. This is because Ar increases over time. However, at a subsequent stage, the continuous spectrum increases more owing to the high temperature and high pressure; therefore, the Ar atomic line spectrum gradually becomes less obvious [Fig. 3(a)]. Figure 3(b) shows that the Ar^+ line spectral changes can be detected near 0.4 μm, which is also within the Eu(II) ion line spectral band. As the energy spectrum of Ar^+ is not as high as that of Eu(II) ions, therefore, it is not shown in Fig. 3(a).

Figure 4 shows how particle number density varies in different regions of the bubble. Owing to the extremely high temperature and pressure conditions inside the bubble, most particles exhibit a peak density at the bubble's core and an abrupt decline near the bubble's wall. The distribution patterns of Ar atoms [Fig. 4(a)] and H_2O molecules [Fig. 4(l)] is different from that of other particles, which is consistent with the inert gas rectification hypothesis that only argon and a small amount of water vapor remain in the bubble.

Additionally, points A–E indicate that both the electron number density and temperature exhibit upward trends [Figs. 2(b) and 4(c)]. In particular, when the bubble reaches its maximum temperature of roughly 16371 K [Fig. 2(b)], the density of the ionized electrons increases considerably to about 4.7096×10^{26} m^{-3} [Fig. 4(c)]. However, this ionization process is accompanied by substantial heat energy consumption, which limits additional temperature increases to some ex-

tent. As the temperature decreases, we observe that the electron number density also declines rapidly. There is a strong positive correlation between the ionized electron density and temperature, which contributes to the short SBSL duration.

To understand the ionization process within the bubble, we also computed the spatial distribution of the ionization energy as well as the degree of ionization and opacity of SBSL at different time points using the method reported in Refs. [24,30] [see Fig. 5]. It was found that ionization mainly occurred during the scintillation stage of the bubbles. When the bubble reached its highest temperature at point D, at the bubble's core, the ionization energy of Ar atoms was substantially lowered to approximately 10.38 eV, surpassing the initial ionization energy of Eu(II), which is approximately equal to 2.95 eV. Given that the standard ionization energy for Ar is 15.8 eV, this indicates a reduction of roughly 34.30% in the ionization energy of the Ar atoms. In addition, we calculated the degree of ionization that represents the proportion of electrons within the bubble relative to the overall count of atoms and molecules present, and found that it was about 5.79%. Throughout the cycle, the maximum ionization occurred in the bubble's core, decreasing abruptly around the bubble's perimeter. The opacity was calculated by multiplying the absorption coefficient (k_λ) with bubble's radius (R).[21] In scenarios where $k_\lambda R$ is considerably greater than one, the spectral line emission is inhibited. Conversely, when $k_\lambda R$ is much less than one, these lines become observable. At the wavelengths of 381 nm and 413 nm, $k_\lambda R$ is approximately one at moment D, making the bubble translucent. During other instances of A, B, C, and E, $k_\lambda R$ is much less than one, rendering the bubble transparent, allowing for the appearance of line emissions (with the exception of moment E owing to the accumulation of spectral radiation).

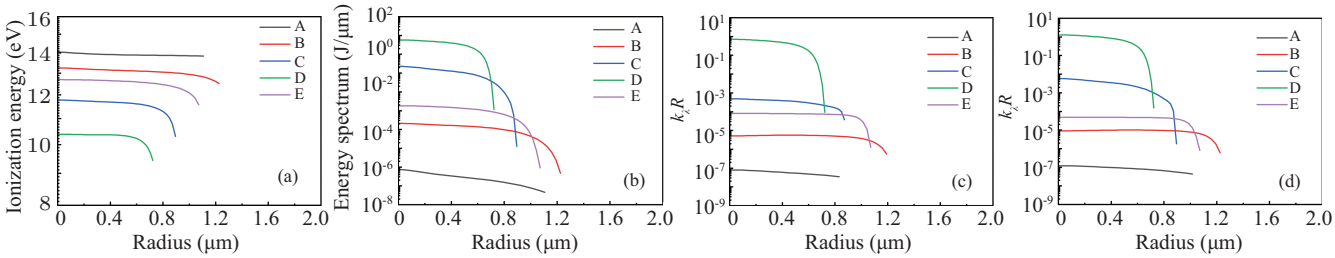


Fig. 5. Spatial distributions of (a) ionization energy, (b) the degree of ionization, (c) $k_\lambda R$ at $\lambda = 381$ nm, and (d) $k_\lambda R$ at $\lambda = 413$ nm in the bubble. The black, red, blue, green, and purple lines correspond to the specific moments A, B, C, D, and E as indicated in Fig. 2(a).

3.2. Spectral characteristics of Eu(II) emission

In order to further explore the characteristics of the Eu(II) emission spectrum of SBSL, we simulated eight driving pressures ($P_{a1}, P_{a2}, P_{a3}, P_{a4}, P_{a5}, \ldots, P_{a8}$) under 0 °C $EuCl_2$ solution of Ar bubbles (see Figs. 6 and 7), where the bubble's original radius is $R_0 = 4.80$ μm and the acoustic drive frequency is 27 kHz. This simulation shows the physical changes inside the bubbles at different driving pressures and the effects of these changes on the Eu(II) emission spectrum.

For simplicity, we treated the $EuCl_2$ solution as a simple water-based treatment in our calculations. The spectral line of the Eu(II) ion in the range of 0.36 μm–0.43 μm is prominent when the minimum driving sound pressure $P_a = 1.2$ atm. The SL spectra of the $EuCl_2$ solution [Fig. 6(a)] at the wavelengths of 372 nm, 381 nm, 390 nm, 393 nm, 397 nm, 413 nm, and 420 nm show peak values, suggesting that the Eu(II) ion underwent ultrasonic decomposition. The continuous spectrum of sonoluminescence is mainly generated by five types of radiation: electron-atomic bremsstrahlung, electron-atom attachment radiation, electron-ion bremsstrahlung, electron–ion complex radiation, and electron-molecular attachment radiation. In contrast, the characteristic spectrum is mainly generated by molecular vibration and rotational radiation, including transition radiation of electrons in atoms and ions. Figures 6(b), 6(c), 7(a), and 7(b) show the simulated distribution of temperature, pressure, ionization energy, and degree of ionization inside the bubble when

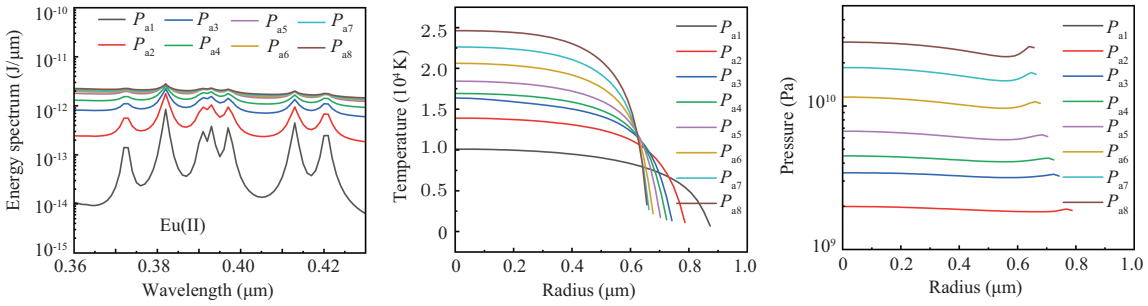


Fig. 6. Ar bubbles in $EuCl_2$ solution driven at 0 °C at eight different pressures, $P_a = 1.2$, 1.25, 1.2731, 1.29, 1.31, 1.34, 1.37, and 1.4 atm, labeled P_{ai} ($i = 1, 2, \ldots, 8$): (a) energy spectrum, (b) temperature, and (c) pressure when the bubble attains its smallest dimension.

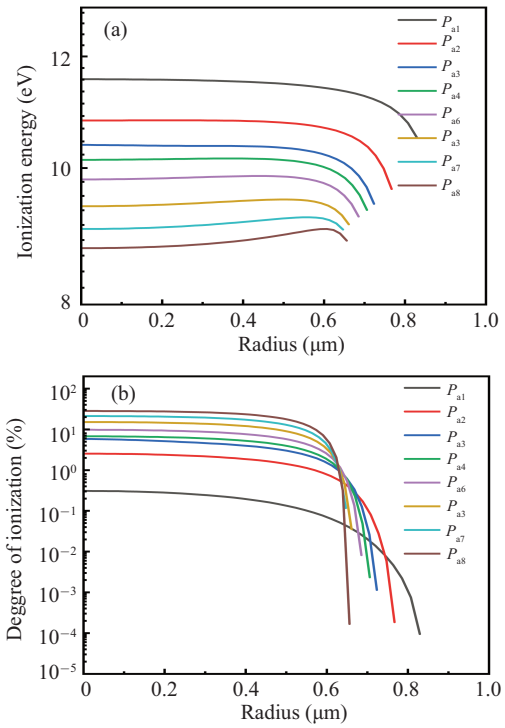


Fig. 7. Ar bubbles in $EuCl_2$ solution driven at 0 °C at eight different pressures, $P_a = 1.2$, 1.25, 1.2731, 1.29, 1.31, 1.34, 1.37, and 1.4 atm, labeled P_{ai} ($i = 1, 2, \ldots, 8$): (a) ionization energy and (b) ionization degree when the bubble attains its smallest dimension.

it attains its smallest dimension under different driving pressure conditions. The temperature, pressure, and degree of ionization inside the bubble were found to be positively correlated with the driving sound pressure P_a, while the ionization energy was inversely proportional to the driving sound pressure. The bubble's core experiences the highest levels of ionization and temperature, while the lowest values are observed at the bubble's wall, with pressure being uniformly distributed throughout the bubble. As shown in Fig. 7(a), at a driving sound pressure of 1.4 atm, the ionization energy for argon atoms at the bubble's core is notably diminished to approximately 8.77 eV, surpassing the initial ionization energy of Eu(II) at around 2.95 eV. Given that the standard ionization energy for argon is 15.8 eV, this suggests a reduction of roughly 44% in the ionization energy of the argon atoms. Figure 7(b) shows that the ionization degree around the bubble's core can reach up to 28.17% at this point, with the bubble reaching a maximum temperature of 24628 K. When the temperature of the bubble core is maintained below about 16371 K, the pressure is about 3.4243×10^9 Pa, and the Eu(II) emission peak stands out from the continuous spectral background in the spectrum. However, as the temperature rises, the Eu(II) emission peak gradually merges into the continuous spectrum and disappears. This suggests that the light emission of the Eu(II) line decreases as the overall brightness of the bubble increases, indicating that sonoluminescent bubbles reaching different maximum temperatures will exhibit different spectral emission profiles.

Both experimental[4,6,30,31] and theoretical[9,21,32] studies have shown that, in single-bubble sonoluminescence, the line spectrum of a dark bubble's light is relatively distinct. As the bubble becomes brighter, both the line emission intensity and the continuous emission intensity increase with rising temperature, but the continuous emission intensity increases at a faster rate. Consequently, the line spectrum gradually becomes blurred or disappears into the background of the continuous spectrum, allowing the continuous spectrum to dominate. This indicates that the spectral characteristics of single-bubble sonoluminescence are closely related to the extreme conditions within the bubble when luminescence occurs.

4. Conclusions

Although the presented calculations cannot fully reproduce all the experimental data, they qualitatively reveal the characteristics of SBSL. Our simulations showed that the characteristic spectra of Eu(II) ions likely originate from the transition radiation of Eu(II) ions when excited under high temperature, pressure, and density conditions. The simulations clearly showed that as the radiation power increased, the Eu(II) ions became gradually blurred and eventually merged into the continuous spectral background until they completely disappeared. Furthermore, the temperature, pressure, and ionization within the bubble all increased as a function of the driving sound pressure, and resulted in a progressively brighter bubble. Consequently, the light emission from the Eu(II) line diminished as the brightness of the bubble increased.

Acknowledgments

Project supported by the National Natural Science Foundation of China (Grant Nos. 12264008, 11864007, and 12204119) and the Basic Research Program of Guizhou Province, China (Natural Science) (Grant No. QKHJC-ZK[2024]ZD054).

References

[1] Gaitan D F, Crum L A, Church C C and Roy R A 1992 *J. Acoust. Soc. Am.* **91** 3166
[2] Flint E B and Suslick K S 1991 *Science* **253** 1397
[3] Lohse D, Brenner M P, Dupont T F, Hilgenfeldt S and Johnston B 1997 *Phys. Rev. Lett.* **78** 1359
[4] Young J B, Nelson J A and Kang W 2001 *Phys. Rev. Lett.* **86** 2673
[5] Brenner M P, Hilgenfeldt S and Lohse D 2002 *Rev. Mod. Phys.* **74** 425
[6] Flannigan D J and Suslick K S 2005 *Nature* **434** 52
[7] An Y 2006 *Phys. Rev. E* **74** 026304
[8] McNamara III W B, Didenko Y T and Suslick K S 1999 *Nature* **401** 772
[9] Liang J F, Xiong D F, An Y and Chen W Z 2022 *Chin. Phys. B* **31** 117802
[10] Tessitore G, Mandl G A, Maurizio S L, Kaur M and Capobianco J A 2023 *RSC Adv.* **13** 17787
[11] Sharipov G L, Gainetdinov R K and Abdrakhmanov A M 2003 *Russ. Chem. Bull.* **52** 1969

[12] Pflieger R, Schneider J, Siboulet B , Möhwald H and Nikitenko S I 2013 *J. Phys. Chem. B* **117** 2979
[13] Sharipov G L, Gareev B M and Abdrakhmanov A M 2010 *JETP Lett.* **91** 566
[14] Liang J F, Chen W Z, Zhou C, Cui W C and Chen Z 2015 *Phys. Lett. A* **379** 497
[15] Liang J F, Chen W Z, Wang X, Yang J and Chen Z 2016 *Phys. Lett. A* **380** 4105
[16] Gareev B M, Abdrakhmanov A M, Yakshembetova L R and Sharipov G L 2023 *J. Appl. Spectrosc.* **90** 9
[17] Gareev B M, Vasilyuk K S, Galimov D I, Sharipov G L and Dzhemilev U M 2020 *Dokl. Phys. Chem.* **494** 147
[18] Sharipov G L, Gareev B M, Vasilyuk K S, Galimov D I and Abdrakhmanov A M 2022 *J. Lumin.* **246** 118859
[19] Gareev B M, Abdrakhmanov A M, Vasilyuk K S, Galimov D I and Sharipov G L 2024 *Appl. Spectrosc.* **78** 125
[20] An Y and Zhang W J 2012 *Chin. Phys. B* **21** 017806
[21] An Y and Li C H 2009 *Phys. Rev. E* **80** 046320
[22] Plesset M S 1954 *J. Appl. Phys.* **25** 96
[23] Keller J B and Miksis M 1980 *J. Acoust. Soc. Am.* **68** 628
[24] Zhang W J and An Y 2015 *Chin. Phys. B* **24** 047802
[25] An Y and Ying C F 2005 *Phys. Rev. E* **71** 036308
[26] Toegel R, Hilgenfeldt S and Lohse D 2002 *Phys. Rev. Lett.* **88** 034301
[27] Kramida A, Ralchenko Y, Reader J and NIST ASD Team *NIST Atomic Spectra Database*, version 5.12, 2025, https://physics.nist.gov/asd
[28] Meyer G, Ruland W, Sahm A and Zu P G 1981 *Astron. Astrophys.* **95** 278
[29] Lang K R 1974 *Astrophysical Formulae: A Compendium for the Physicist and Astrophysicist* (Berlin, New York: Springer) pp. 208–217
[30] Yasui K 2001 *Phys. Rev. E* **64** 016310
[31] Chen W Z, Huang W, Liang Y, Gao X X and Cui W C 2008 *Phys. Rev. E* **78** 035301
[32] An Y and Li C H 2008 *Phys. Rev. E* **78** 046313